Wireless Bicycle Assist: Structural Analysis of Outer Casing

by

Kashika Sharma

SUBMITTED TO THE DEPARTMENT OF MECHANICAL ENGINEERING IN PARTIAL FULFILLMENT OF THE REQUIREMENTS FOR THE DEGREE OF

BACHELOR OF SCIENCE IN MECHANICAL ENGINEERING
AT THE
MASSACHUSETTS INSTITUTE OF TECHNOLOGY

ARCHIVES

MASSACHUSETTS INSTITUTE OF TECHNOLOGY
SEP 16 2009
LIBRARIES

JUNE 2009

© 2009 Kashika Sharma. All rights reserved.

The author hereby grants to MIT permission to reproduce and to distribute publicly paper and electronic copies of this thesis document in whole or in part in any medium now known or hereafter created.

Signature of Author:.....
Kashika Sharma
May 8, 2009

Certified by:.....
Julio Guerrero
Lecturer in Mechanical Engineering
Thesis Supervisor and Reader

Accepted by:.....
John. H. Lienhard V
Professor of Mechanical Engineering
Chairman, Undergraduate Thesis Committee

Wireless Bicycle Assist: Structural Analysis of Outer Casing

by

Kashika Sharma

Submitted to the Department of Mechanical Engineering
on May 8, 2009 in partial fulfillment of the
requirements for the Degree of Bachelor of Science in
Mechanical Engineering

ABSTRACT

Although cost effective and environmentally friendly, bicycles are impractical for many users due to the required strength and physical exertion. The GreenWheel is a set of mechanical and electronic devices that provide adjustable amounts of torque to a bicycle wheel to assist the rider in pedaling. This device makes bicycles accessible to a much larger fraction of the population.

The device consists of two main modules, one of which is mounted on the handlebar, allowing the user a convenient way to set a desired torque output. It functions to wirelessly convey this information to the second main module, which mounts at the center of the rear wheel of the bicycle and is designed to exert a user-desired amount of torque to the wheel. The inner portion of this module contains a motor layout, including batteries, solenoids, and magnets. The outer portion of this module is a casing that rotates on bearings on the bicycle shaft. It is held in place by the spokes of the wheel that attach to the holes at the circumference of the device. Originally the device was designed to operate using brushed DC motors. Realizing the potential of brushless DC motors, brushed DC motors were abandoned in the design of the actual product that will be released in the market. This change required a complete redesign of the inner casing that stored the motor. This also created the need to redesign the outer casing to provide the device with the proper structural integrity and a more appealing and elegant design. This thesis focuses on the redesign of the outer casing, the analysis of its two critical components, and its aesthetics.

One of its two critical components is the material of spoke-holes on the circumference of the outer casing to which the spokes will be attached. It was evaluated for the amount of shear that it will experience as a result of spoke tension. The second critical component is the material of the bicycle shaft to which the motor was attached. It was analyzed to prevent failure from shearing due to the electromagnetic forces created by the motor coils. In addition, aesthetics and ease of assembly and servicing were also considered in the design of the device.

The area of the outer casing that surrounds the spoke-holes was analyzed using the largest amount of force that it will experience from the spokes. It was found that these areas that surround the spoke-holes are strong enough to withstand the shear stress from the spokes. The shaft was designed to withstand the torsion generated during the operation of the motor.

Thesis Supervisor: Julio Guerrero
Title: Lecturer of Mechanical Engineering

1. INTRODUCTION

GreenWheel is an electronic bicycle assistive device that provides an adjustable amount of torque to the rear wheel of the bicycle. This device consists of a motor component that can be mounted to the rear wheel of any bicycle and a rotator switch, which is mounted onto the handlebar. The switch provides the user with an easy way to control their assisted speed. The switch includes a wireless transmitter that communicates with the motor to adjust the torque output.

The GreenWheel device was created by Arthur Petron, a graduate student at the Mechanical Engineering at Massachusetts Institute of Technology. Originally, the device was operated by a brushed DC electric motor. Although this type of motor is simple and easy to design around, it was decided that it is not best for fulfilling the GreenWheel project's design requirements, see Table 1 for detailed engineering requirements. As a result, a decision was made to design a new motor for the rear wheel module: a brushless DC torque motor.

Short Name	Definition
Maximum Torque	The motor must exert 60Nm of torque to the rear wheel of the bicycle.
Aesthetically Pleasing	• Design of the rear wheel module must be consistent with the design of most bicycles. • Rear wheel module must not protrude past the frame of the bicycle
Wireless communication	The handlebar module must be able to wirelessly communicate with the rear wheel module. Windows must be installed in the outer casing of the rear wheel.
Robust	• The installation and operation of device does not compromise safety and stability of the bicycle • The modules must withstand harsh environments and weather to a similar degree as the rest of the bicycle's components.
Ease of Use/Installation	• The device must be easy to install and operate. • The battery installation must not require taking the rear wheel module apart from the bicycle frame.

Table 1. Design requirements for GreenWheel.

A brushless motor offers multiple advantages over a brushed motor. It is more efficient, less noisy, longer lasting due to the lack of brush erosion, and is less susceptible to electromagnetic interference. In addition, the electromagnets are attached to the outer casing of the motor and can be cooled by conduction between the magnets and the material of the outer casing, thereby requiring no airflow within the casing. This enables all the components to be entirely enclosed within the casing, preventing dust and moisture from coming into contact with the electronic components. Although this type of motor is not as widely used as a brushed motor, overall it is a much better choice for GreenWheel since it is much more robust and has more desirable characteristics.

The decision to create a new motor resulted in the need to redesign the inner layout of the motor casing since a brushless motor has different components and requirements. The new casing design has two critical components that are analyzed in this paper to prevent them from failing during bicycle operation: 1) the spoke holes around the circumference of the device that are used to attach the casing to the spokes, and 2) the shaft around which the outer casing rotates. The redesign also provided the opportunity to redesign the outer casing to make it more visually appealing. Consideration had to be given to the geometric constraints of the motor components and the bicycle frame. See figure 10 for details about the components of the rear wheel module.

2. DESIGN FOR MECHANICAL PROPERTIES

This section highlights the analysis of the two critical components of the rear-wheel module: 1) the area surrounding the spoke-holes, and 2) the shaft that the motor rests on.This section has three subsections. The first one, a, describes the forces on a wheel that comes into contact with a bump while moving at a certain velocity. The second and third sections, **b** and **c**, present the analyses of the spoke-hole component and the shaft component, respectively.

a. Forces associated with a Bump

This section is based on Petron **[1]**. The largest forces on the device will occur when the maximally loaded bicycle is moving at maximum speed and rides over a specified maximum bump size. It is therefore useful to evaluate these forces in order to understand the most likely failure mode for the device. Figure 1 shows a free-body diagram for the rear-wheel of the bicycle riding over a bump of given height.

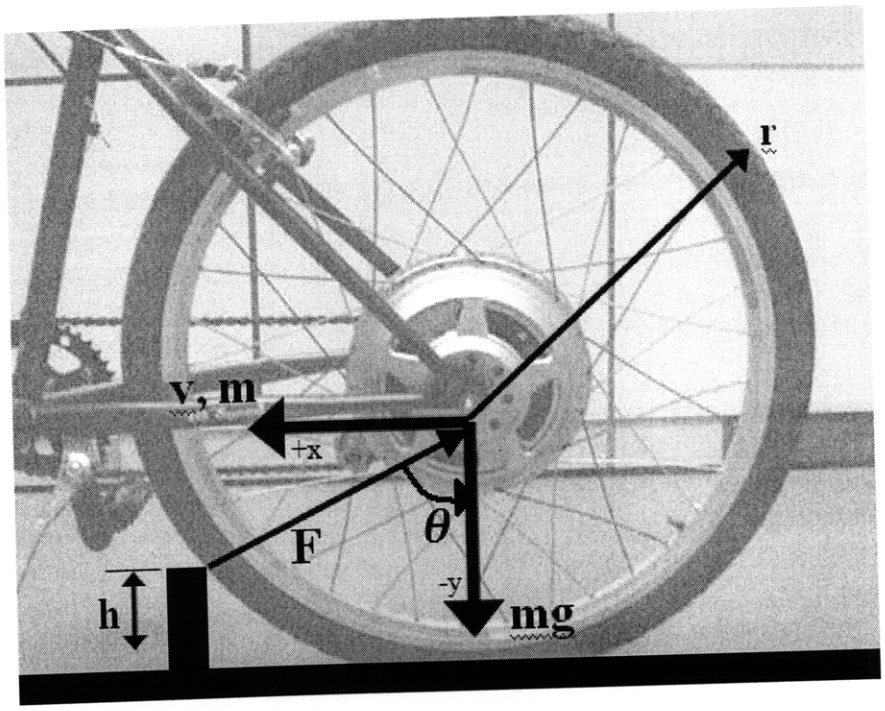

Figure 1: Free-body diagram of the rear wheel of a bicycle of radius, r, as it goes over a bump of height, h, traveling at a velocity, v.

Riding the bicycle on a smooth road creates a force, F, of approximately 1 times the force of gravity on the device. However, since riding the bicycle over a bump causes an upward, lifting force and a backward, stopping force on the wheel whose combined effect is much greater than

the force caused by riding the bicycle on a smooth road, these are the forces considered significant in the analysis of the device (Figure 1).

The angle at which the bump-force acts, θ, on the device is described as

$$\theta = \frac{\pi}{2} - \sin^{-1}\left(\frac{r-h}{r}\right). \tag{1}$$

This angle is calculated between a vertical line from the center of the device and a line from the impact point to the center of the bicycle. In other words, the force vector is perpendicular to a line tangent to the wheel at the point of impact. Using this definition of theta, the upward force on the wheel can be calculated as

$$F_y = 1 + \upsilon \cos\left(\frac{\pi}{2} - \theta\right), \tag{2}$$

where v is held constant and equal to the maximum velocity. The force in the x-direction can then be expressed as

$$F_x = F_y \tan(\theta). \tag{3}$$

Figure 2 shows the non-dimensional ratio of force to total weight of the bicycle in the x- and y-directions as a function of the dimensionless parameter h/r. In the plot, the data for the ratio of force in the y-direction was obtained by using the maximum value for the velocity, v, in equation 2. The data for the ratio of force in the x-direction was obtained by substituting equation 2 into equation 3. The data for ratio of total force was determined by parametrically combining equations 2 and 3.

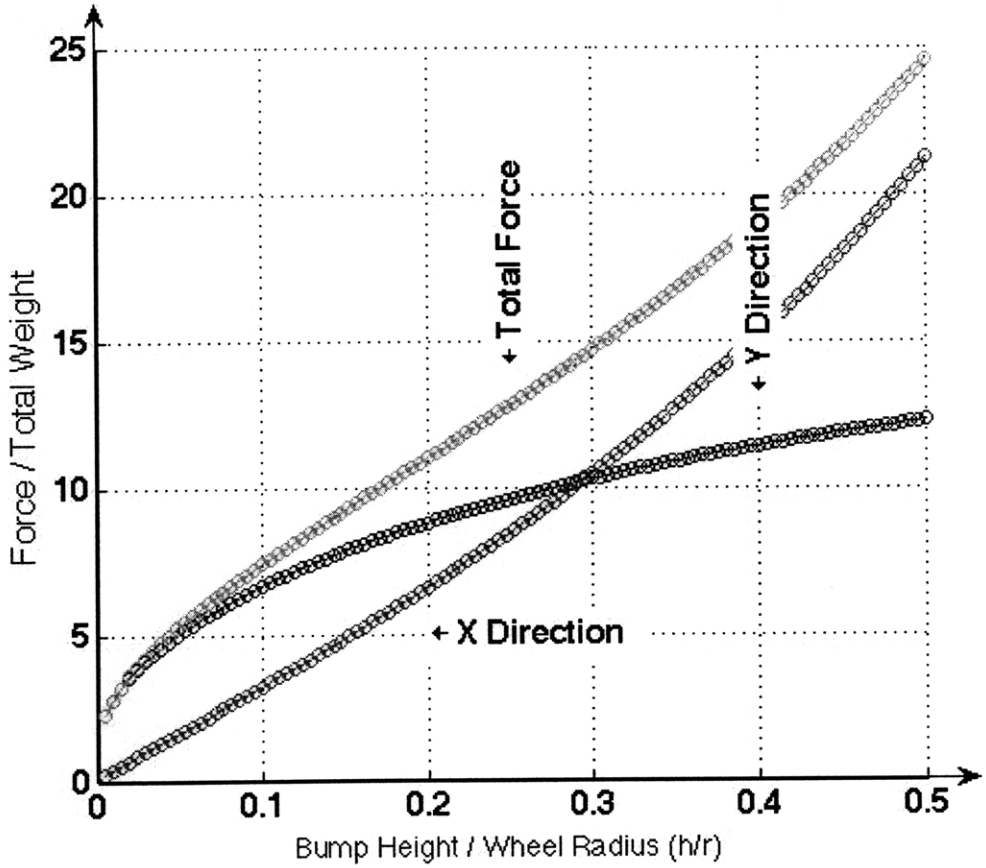

Figure 2: The forces (in g's) on a wheel of radius r in the x- and y-directions. Notice how the force in the x-direction approaches infinity as h/r increases (Petron, 2008).

Note that as the bump height approaches the radius of the wheel, the force in the x-direction approaches infinity.

b. Spoke-Hole Analysis

i. Shear Theory

The GreenWheel motor is mounted to the rear wheel of the bicycle and the spokes of the wheel are attached to spoke-holes around the circumference of the device, as shown in Figure 1. Since the spokes can only withstand tension, only the spokes at the top exert load on the housing. The bottom spokes do not exert loads. As a result, the spokes at the top tend to shear the material surrounding the holes where they are mounted. Upon loading, only the top half of the wheel

experiences stress. The largest force on the spokes will occur when a maximally loaded bicycle is moving at maximum speed and travels over a bump.

A shear analysis is performed to ensure that the material around the spoke-holes do not fail from spoke tension. The hole supporting the vertical spoke is used in this analysis since it experiences the most tension. The spoke will rest at the upper edge of the hole (Figure 3a) and cause a stress above its outer edge in a direction perpendicular to the line tangent to the top of the hole. As a result, it can be assumed that the stress is applied at the edge of the casing instead.

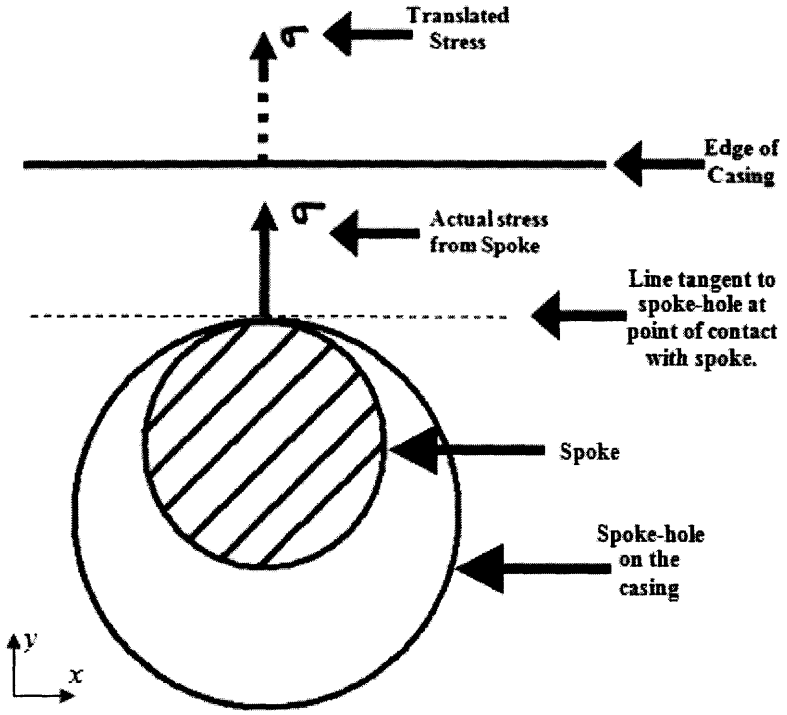

(a)

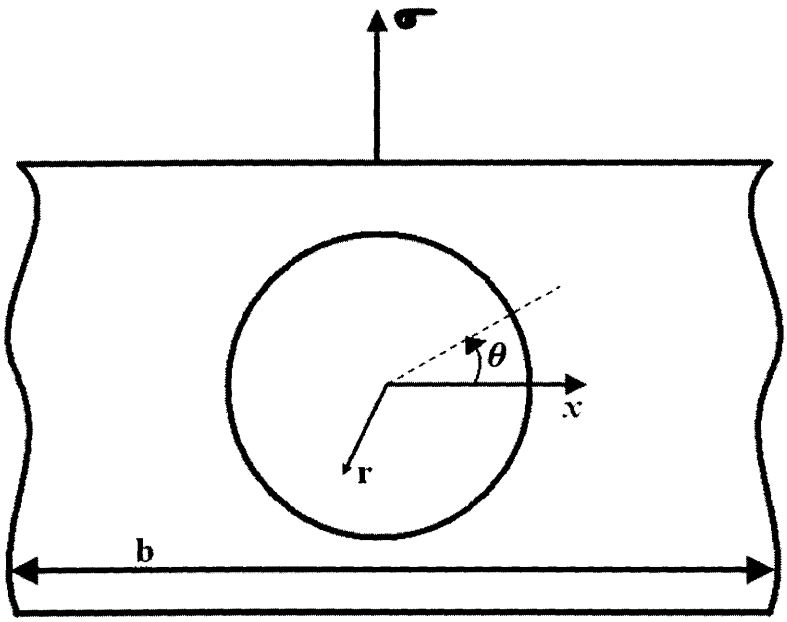

(b)

Figure 3: (a) Representation of the spoke resting against the top edge of the spoke-hole. Note that since the spoke causes stress at the top edge of the hole, the same stress can be translated to the outer edge of the casing. (b) Model of the spoke and hole as a thin, remotely loaded plate with geometric discontinuity.

Therefore, this scenario must be analyzed as a thin plate with a circular hole.

To simplify the analysis, it can be assumed that the plate has an infinite height. This follows the logic described above where since the stress is applied at the top of the hole, it can be assumed that the stress is applied to the plate at any distance from the hole.

St. Venant's Principle states that the effects of stress field concentrations due to geometric discontinuity, i.e. hole of diameter $2a$, are only significant within a distance of three times the characteristic linear dimension of the discontinuity. The effect of the stress field decreases as the distance, along b in Figure 3b, from the hole increases and becomes insignificant at a distance three times the diameter from the left and right edges of the spoke-hole. Figure 4 presents an example of this concept. It shows a map of the stress field concentration around a thin plate with a hole at its center that is loaded with a tension of 25kN at

its top and bottom. The x and y axes indicate the length of the plate in meters. The colors in the figure correspond to different magnitudes of stress in the plate and their approximate values can be determined using the color-scale at the right. It can be seen that the stress values are highest at the left and right edges of the hole and are approximately three times the magnitude of the applied stress. At a distance of approximately three times the diameter of the hole, the stress magnitudes are similar to the applied stress on the plate.

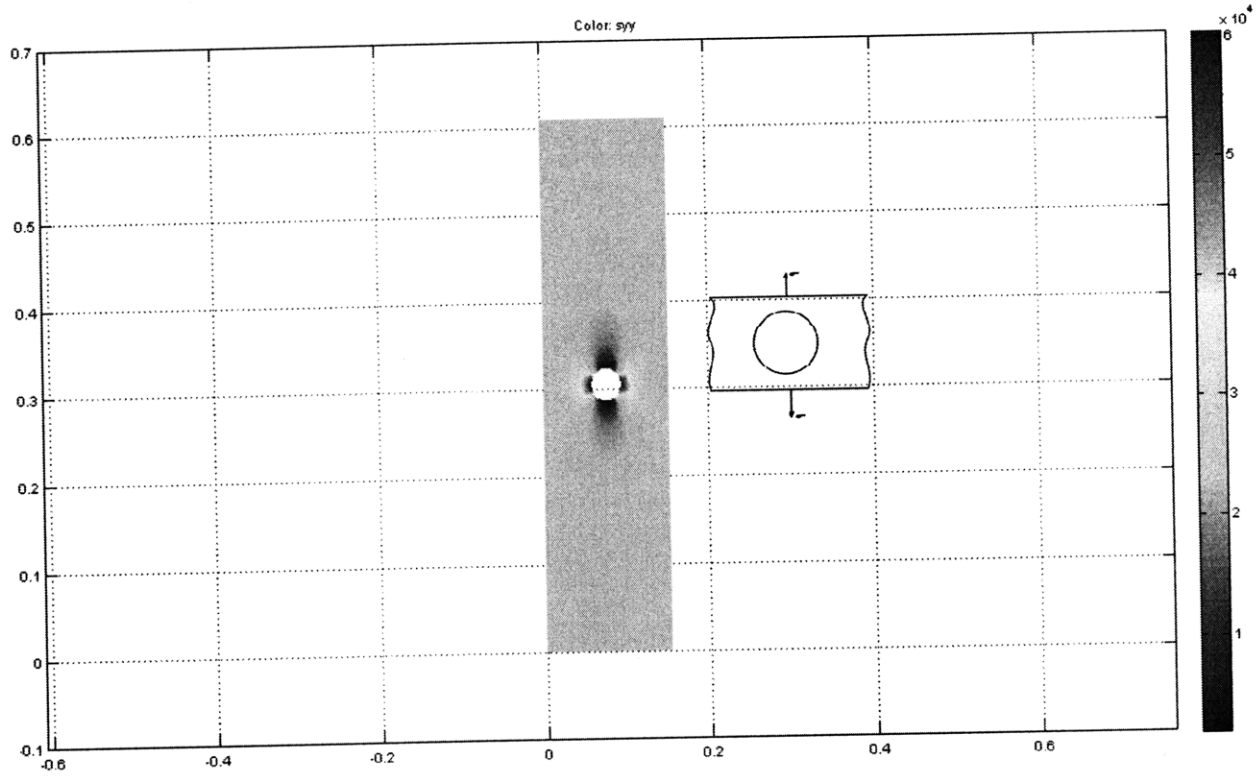

Figure 4: Map of stress field concentration as a thin plate with a hole at its center is loaded with tension of 25kN at its top and bottom. Note that this is only an example to aid in understanding of the analysis presented here. This does NOT represent the spoke-holes contained in the device.

As can be seen in Figure 4, the stress field concentration effects are negligible at a significant distance from the hole. Since the holes in the device are 3 mm in diameter and are spaced 47mm apart, it is reasonable to assume that there are no effects on the stress field concentration at each hole due to other holes in the device. As a result, each hole may be analyzed independently.

For a thin-plate of given width and infinite height with a circular hole, the overall stress distribution in the plate is described in Hibbeler [2] as,

$$\sigma_{rr}(r,\theta)=\frac{\sigma}{2}\left[\left(1-\frac{a^2}{r^2}\right)+\left(1+3\frac{a^4}{r^4}-4\frac{a^2}{r^2}\right)\cos(2\theta)\right], \tag{4}$$

$$\sigma_{\theta\theta}(r,\theta)=\frac{\sigma}{2}\left[\left(1+\frac{a^2}{r^2}\right)+\left(1+3\frac{a^4}{r^4}\right)\cos(2\theta)\right], \tag{5}$$

$$\sigma_{zz}(r,\theta)=\frac{\sigma}{2}\left[\left(1-3\frac{a^4}{r^4}-2\frac{a^2}{r^2}\right)\cos(2\theta)\right], \tag{6}$$

where the edge of the circular hole is located at $r = a$. It is important to note that this analysis assumes planar stress in which the thickness of the plate is less than or equal to the radius of the hole). At $r = a$,

$$\sigma_{rr}(r,\theta)=\sigma_{zz}(r,\theta)=0 \tag{7}$$

$$\sigma_{\theta\theta}(r,\theta)=\sigma(1-2\cos(2\theta)). \tag{8}$$

The hoop stress, $\sigma_{\theta\theta}$, at $\theta = +/- \pi/2$ has a maximum value of

$$\sigma_{max}=3\sigma. \tag{9}$$

Figure 5 shows the hoop stress felt by the material at the boundary of a spoke-hole.

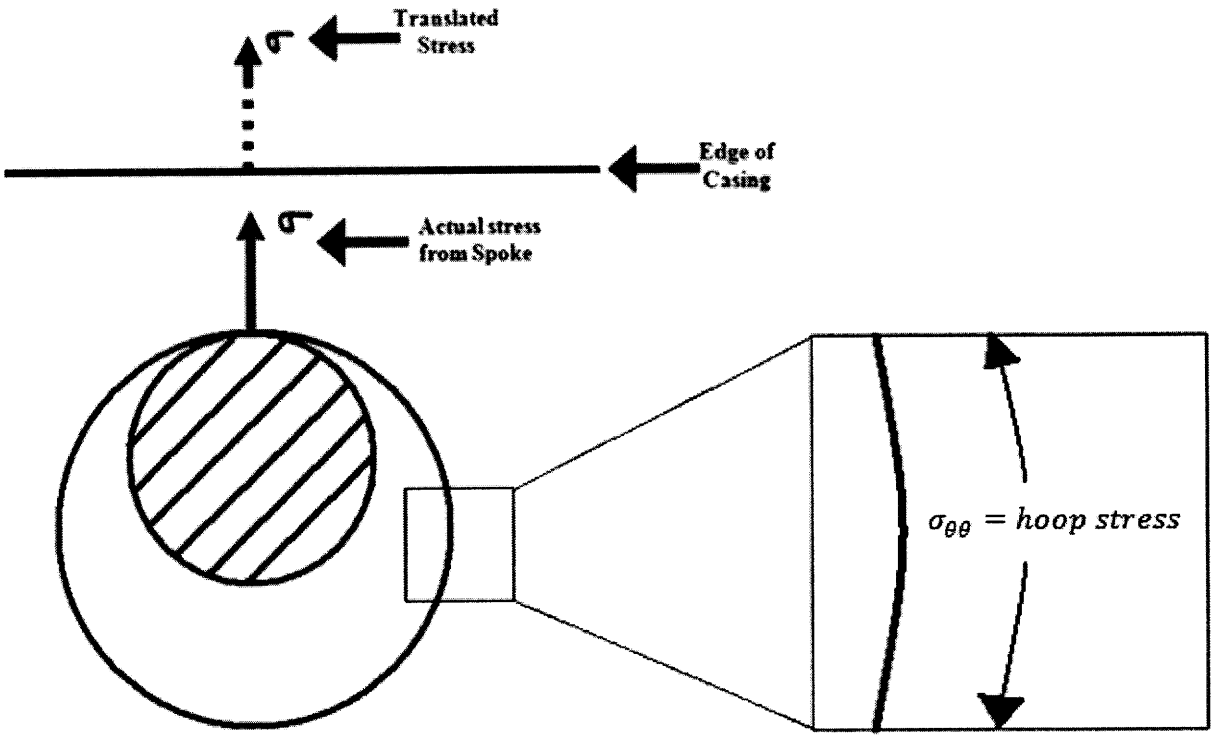

Figure 5: A representation of the spoke-hole depicting hoop stress, $\sigma_{\theta\theta}$, on the material around its edges.

It is important to note that the hoop stress at the two edges of the hole is far greater than the far-field stress. The far-field stresses will be equal to the actual stress imposed on the hole by the spoke. As a result, remote stress that is small enough to not cause any failures in regions farther away from the hole, may initiate failure locally at the edges of the hole.

To prevent failure of the spoke-holes, the maximum stress caused within the hole should be less than the yield strength of the material. To ensure safety, a safety factor of 2 is used in equation 10 to determine the maximum stress that can safely be exerted on the spoke-holes to prevent failure by shearing:

$$\sigma_{\max} < 2 \times \sigma_{yield} . \quad \textbf{(10)}$$

Since the maximum stress is the localized stress at the two edges of the spoke-hole, the remote stress caused by the spoke can be determined using Equation 9. It can also be expressed as

$$\sigma = \frac{F_{spoke}}{A}, \tag{11}$$

and can be used to find the maximum force that can be exerted by the spoke before failure occurs. This data is summarized in Table 2 (Matweb [3]).

Yield Stress of 6061-T6 Aluminum	276 MPa
Maximum allowable stress (safety factor=2)	138 MPa
Maximum allowable force	6.6 kN

Table 2: Calculated values for the maximum allowable spoke force and the maximum bump size that the bike can ride over while moving at its maximum velocity. 50 km/hr (30mph).

ii. Bicycle Specifications

Table 3 shows the driving specifications for a bicycle using GreenWheel assist. The working load is the sum of weights of the bicycle and the rider. The maximum speed is the fastest speed at which the bicycle can operate using GreenWheel. The maximum bump size represents the maximum height of a curb. The maximum stress that the vertical area around the vertical spoke-hole can withstand is calculated using the mentioned specifications and the analysis presented in section **1.a.i**.

Working Load	120 kg
Maximum Speed	30mph (50km/hr)
Maximum bump size	4 in (101.6 mm)
Maximum stress on vertical spoke-hole	184 MPa

Table 3: Driving specifications for a bicycle using GreenWheel.

The maximum stress on the area around the vertical spoke-hole boundary of a maximally loaded bicycle moving at maximum speed is slightly greater than the allowable maximum stress, with a safety factor of 2, but still much less than the yield stress of the Aluminum alloy. It is also important to note that this is the extreme case, most likely an accident, since one will most likely approach a bump of this size with a much slower speed (~5mph) and cause a much lower stress on the spoke-holes.

c. **Bicycle Shaft Analysis**

i. **Torsion Theory**

The motor of the rear wheel module is stationary with respect to the frame of the bicycle and is attached to the shaft of the wheel. As the outer casing rotates on the bearings, the electromagnetic field between the coils of the motor and the magnets on the outer casing imposes a distributed moment on the shaft. Figure 6 presents a simplified representation of this system, showing key parts such as the bearings that the outer casing rotates on, the motor that represents the inner casing that rests on the shaft, and the outer casing. The frame of the bicycle acts as ground for the shaft.

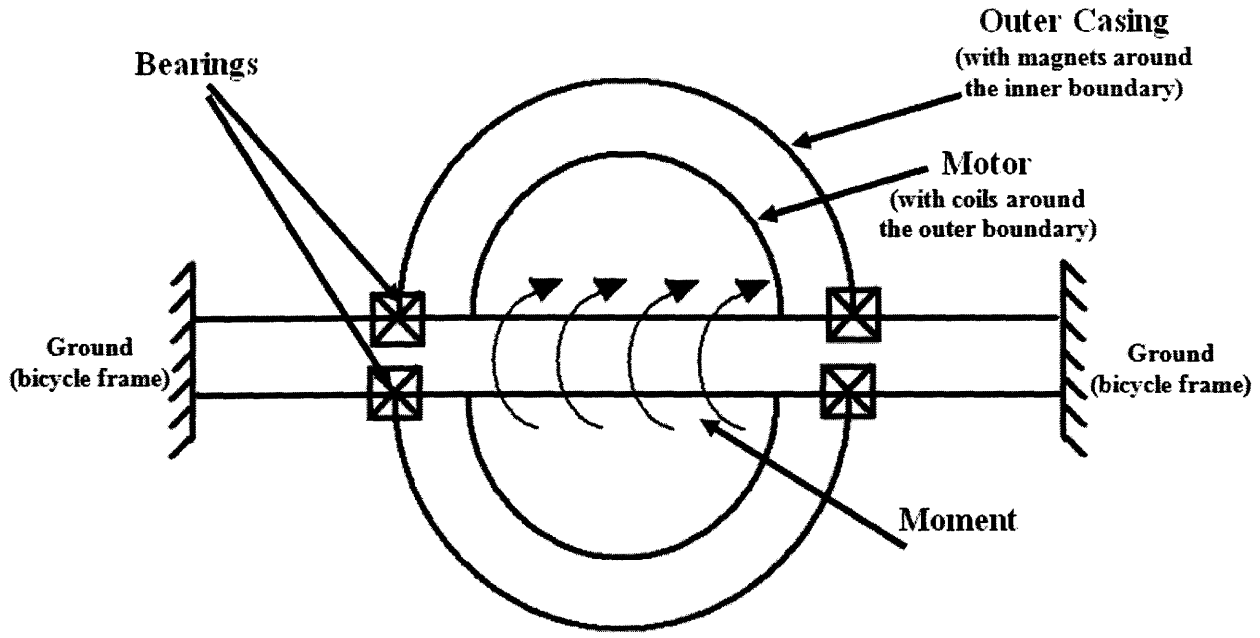

Figure 6: Simplified representation of the outer and inner casings and the shaft. Note that the shaft is grounded by the bicycle frame.

This moment can be analyzed by modeling the shaft as a solid, cylindrical shaft, made of linear elastic material, that is constrained at both ends with no degrees of freedom by the bicycle frame (Figure 7).

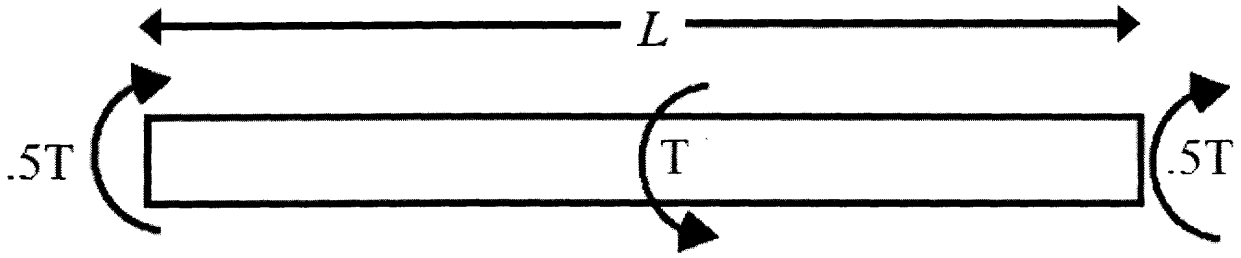

Figure 7: A free-body diagram illustrating the torque that the shaft experiences.

Total shear on the shaft is expressed in equation 12, where average shear is calculated using equation 13 (Hibbeler [2]):

$$\tau_{Total} = \tau_{z\theta} + \tau_{Avg}, \tag{12}$$

$$\tau_{Avg} = \frac{Load}{A_{Cross-Sectional}}. \tag{13}$$

Since the moment distribution is symmetrical about a vertical axis at the middle of the shaft, the maximum shear force can be found by analyzing a radial cross-section of the shaft (Figure 8).

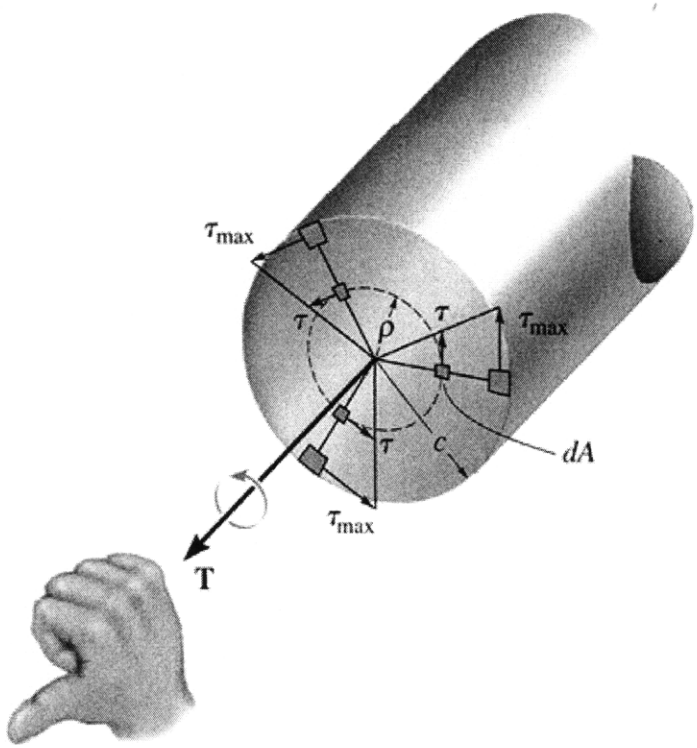

Figure 8: Shear stress varies linearly along each radial line of the cross section (Hibbeler, 2005)

The shear torque can be described as shown in equation 15, as inferred from Hooke's Law,

$$\tau = \left(\frac{\rho}{c}\right)\tau_{\max}. \tag{14}$$

Equation 14 represents shear stress as a function of radial position, ρ. Note that the shear stress in the cross-section increases linearly in the outward radial direction on the shaft. Equilibrium analysis on the shaft results in torque in the entire cross-section, expressed as (Hibbeler [2]),

$$T = \int \rho T dA = \tau_{\max} c \int_0^c \rho^2 (2\pi \rho d\rho). \tag{15}$$

Since maximum shear occurs at the outer edge of the shaft, plugging in c = D/2 in Equation 15 and solving for maximum shear results in

$$\tau_{\max} = \frac{32T}{\pi D^3}. \tag{16}$$

Substituting Equations (13) and (16) into Equation (12) results in the total shear stress on the shaft:

$$\tau = \frac{Load}{A_{Cross-Sectional}} + \frac{32T}{\pi D^3}. \tag{17}$$

ii. Tresca Yield Criterion

In 1968, Henri Tresca proposed the maximum-shear-stress theory that predicts the failure criteria for ductile materials, such as the one that the shaft is made of. The theory explains that if absolute maximum shear stress reaches the value of shear stress that causes the material to undergo yielding when it is subjected to only axial tension, yielding of the material will occur. For application, the absolute maximum shear stress is expressed in terms of principle stress, σ_{max}. Therefore, to prevent failure (Hibbeler [2]),

$$\tau \leq \frac{\sigma_{yield}}{2}. \tag{18}$$

The shear force calculation of a maximally loaded shaft, 0.5 inches in diameter, as a result of maximum motor torque, 60Nm, calculated using equation 17 results in 299MPa. Some materials that the shaft may be made of are listed in Table 4, along with their yield strength values, divided by a safety factor of 2 (Matweb [3]). They are divided by two to coarsely approximate their maximum shear stress to half their yield stresses.

Material	Yield Strength/2 (MPa)
High Carbon Steel	1375
Low Carbon Steel	1200
Stainless Steel	695
Low Alloy Steel	370
Medium Alloy Steel	695

Table 4. Potential Materials of bicycle shafts and their respective yield strengths.

Table 4 indicates that all the potential materials that a bicycle shaft can be made of have maximum shear stress that is greater than the calculated shear force that the motor will exert on the shaft. This indicates that the material of the shaft will not fail due to motor torsion.

3. GEOMETRIC/OPERATIONAL CONSTRAINTS

Certain design constraints were taken into consideration while designing the outer casing for the motor in the rear wheel module of the GreenWheel. The design of the new casing for the motor is meant to be device driven; it is designed to be mounted onto the rear wheel of any bicycle without modifying its rear frame. In other words, the outer casing of the rear wheel module must be able to fit within most bicycle frames. The design is also user-driven; it must be easy to install and easy to operate. Keeping this in mind, the rotator switch was designed to be mounted onto the handlebar so the rider can access it using his thumb with minimal effort, without having to remove his hand from the handlebar.

Certain operational features also influenced the design of the outer casing. For example, wireless sensors within the casing must have a way to communicate with the transmitter on the handlebar. The signals sent from the transmitter would not be able to pass through the outer casing magnets due to the electromagnetic field created by the motor coils or through the aluminum casing material. As a result, window slots are incorporated on one side of the casing and plastic windows are designed to be fitted into the slots. Rubber gaskets are placed between the plastic windows and the slots in the casing to make the windows water- and dust-proof.

Another operational feature that was important towards the design was the ease of charging and replacing the batteries within the casing. Consequently, the casing was designed in three parts: two outer sections and a middle section that keeps the outer sections together using bolts, see figure 9.

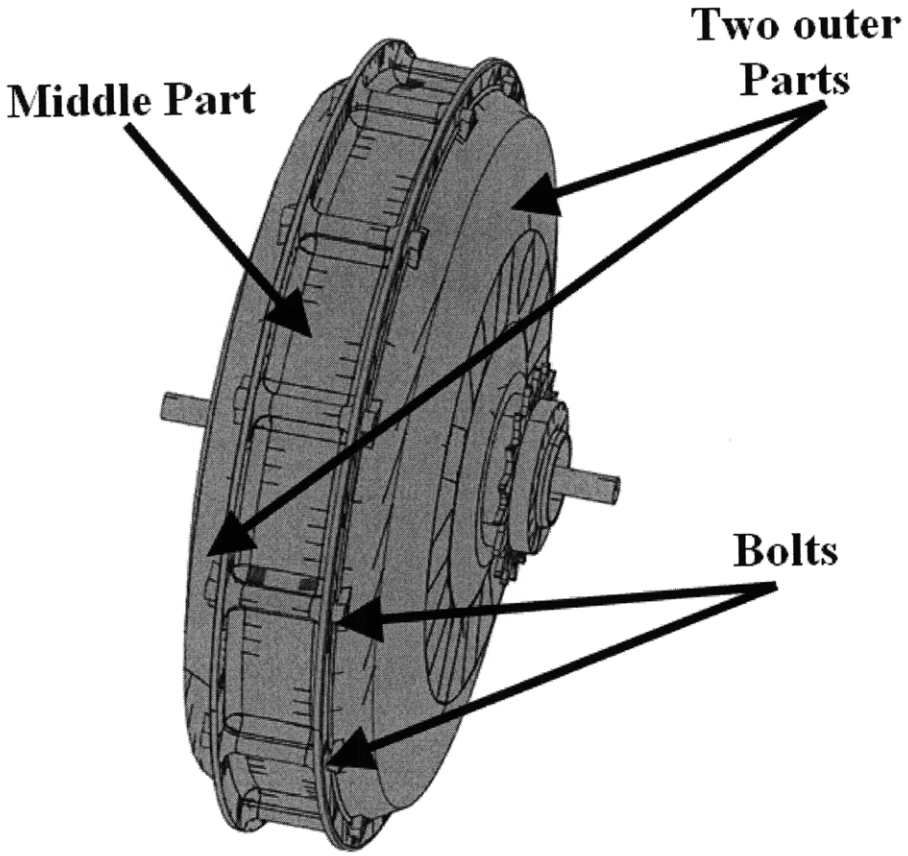

Figure 9: A 3-D model of the final design of the casing. The two outer parts of the casing are held together by the middle section using bolt screws.

In the case that the user needs to replace batteries located inside the device, one of the two side plates can easily be removed by unbolting the screws to reveal the batteries inside. This eliminates the need to dismount the entire motor device from the wheel to replace or service an inner component. Furthermore, a USB charge port has been added to the casing that can be plugged into a computer for charging or can be plugged into a wall through a converter.

4. AESTHETICS DESIGN

The GreenWheel has also been designed to enhance the features of a regular bicycle while maintaining elegance. The wireless feature eases the installation process and eliminates external wiring running from the transmitter on the handlebar to the motor on the rear wheel. All the components of the device are compactly stored within the motor casing, including the batteries that power the device, eliminating the need to install large battery packs. These considerations contribute to an aesthetically pleasing design as shown in Figure 9. An exploded view of the outer casing, along with the inner layout, is presented in Figure 10. Table 4 lists the part names to assist with the labeling in Figure 10.

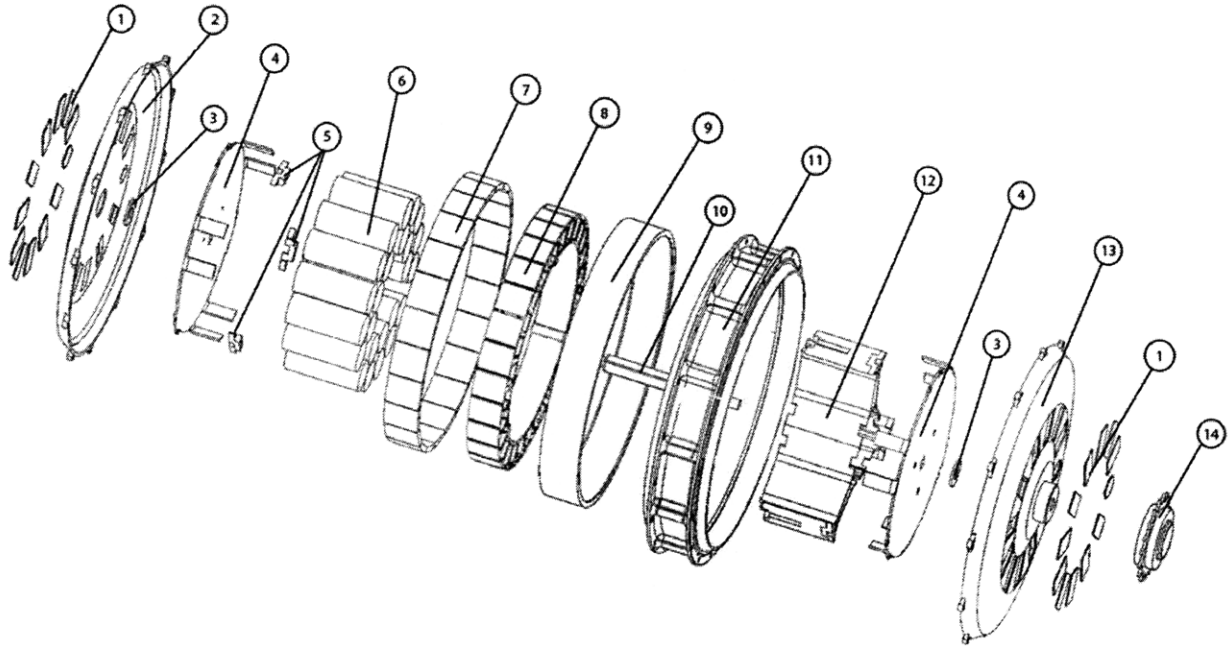

Figure 10: Exploded diagram of the second module.

Part Number	Part Name
1	Windows
2	Outer Casing
3	Bearing
4	Battery Cover Plate
5	Stator Locking Mount
6	Battery Assembly
7	Magnets
8	Stator
9	Rotator
10	Shaft
11	Central Outer Casing
12	Internal Support Structure
13	Outer Casing
14	Freewheel

Table 4: Names for the parts labeled in Figure 10.

5. FUTURE TASKS

Before the product can be brought to market, further tasks need to be completed. One important task that still requires more work is testing the device to ensure proper function and safety of the user. The device is designed to be waterproof; it must be tested for this feature to ensure the electronic components within the casing do not come into contact with any moisture. A standard for describing the waterproofing level of the device must be established to indicate whether the device is waterproof simply in rainy weather or whether it can withstand being submerged in water.

Another area that needs to be tested is making the installation simple and easy to follow. Installation manuals need to be created and tested among users. They must be able to follow the instructions with minimal confusion. Another way to solve this problem is by forming contacts with bicycle maintenance stores and directs the users to these stores to have their devices installed correctly at small costs.

In addition, there are some electronic features that must also be tested to ensure their reliability. In the case that communication between the transmitter and the motor fails, the user

must be able to regain full control of their bicycle. Furthermore, the motor has been designed such that if it does not receive data from the transmitter, it will simply stop working and the electric bicycle will resort to functioning as a regular bicycle so that the user can continue pedaling. These functions must be tested to ensure the reliability of proper functioning of the bicycle.

6. CONCLUSION

The GreenWheel promises to overcome many barriers to the widespread use of bicycles. The recent redesign of the device components satisfies the design requirements for the project more completely. As part of the redesign process, a new outer casing for the rear module of the device was designed. The analysis and explanations presented in this study support the decisions that were made in the design of this component. As such, the goals of this project outline in section 1 were fulfilled.

References:

[1] Petron, A., "The Folding Roboscooter: Structural Analysis for an Electric Scooter used in Urban Conditions." MIT Thesis. 2008

[2] Hibbeler, R.C., "Mechanics of Materials" Pearson Prentice Hall 2005

[3] Materials Specifications "*MatWeb* – The Online Materials Information Resource" www.matweb.com 2008

Acknowledgements:

Julio Guerrero. Lecturer of Mechanical Engineering
Alex Slocum. Professor of Mechanical Engineering
Rick Slocum. Lecturer of Mechanical Engineering
David M. Parks. Professor of Mechanical Engineering
David Custer. Writing Instructor and Lecturer of Experimental Study Group
Nikolai Begg, Candidate of Bachelor of Science in Mechanical Engineering
Arthur Petron. Candidate of Masters in Mechanical Engineering
Joshua Siegel. Candidate of Bachelor of Science in Mechanical Engineering